Available online at www.sciencedirect.com

ScienceDirect

Procedia Chemistry 00 (2011) 1–20

Procedia Chemistry

22nd Solvay conference in Chemistry

Quantum field, interference, and entanglement effects in nonlinear optical spectroscopy

Shaul Mukamel and Yuki Nagata

Department of Chemistry, University of California, Irvine, Irvine, CA 92697

Abstract

Experimental observables in quantum systems may be represented by *Liouville space pathways* which describe the evolving density matrix. The pathways of coupled degrees of freedom may become entangled leading to interesting interference effects. We demonstrate and classify signatures of these quantum effects in optical measurements which involve both classical and quantum modes of the radiation field. Generalized response functions recast in terms of superoperators are used to provide a compact unified description of a broad range of measurements. We discuss interferences of quantum pathways of matter related to the entanglement of excitons in chromophore aggregates, and how they can be manipulated by interactions with quantum optical fields.

Keywords: ultrafast spectroscopy, coherence, quantum optics, entanglement, quantum fluctuations, excitons

1. Quantum pathways for observables

All quantum effects on dynamics are ultimately associated with interference among pathways. This is clearly seen in the Feynman path formulation of the evolution of the wavefunction in space-time [1]. Usually, the wavefunction is not an experimental observable (quantum tomography and quantum information algorithms are exceptions) [2, 3, 4, 5, 6]. Common dynamical observables are given by expectation values of operators which contain less than the complete information carried by the wavefunction. These can be represented by *Liouville space pathways* which describe the joint evolution of the bra and ket and represent the system's density matrix [7, 8]. When two or more systems are coupled, their pathways become entangled and this leads to new and interesting quantum effects. In these notes, we survey these interference effects as they show up in nonlinear optical spectroscopy.

We start with the quantized light-matter Hamiltonian in the interaction picture with respect to the optical field[9]

$$H(t) = H_0 + H'(t), \tag{1}$$

where H_0 is the matter Hamiltonian, and $H'(t)$ is the field-matter dipole coupling given by

$$H'(t) = -\sum_{\alpha} E'_{\alpha}(t) V'_{\alpha}. \tag{2}$$

The quantized electric field of mode α is given by

$$E'_{\alpha}(t) = E_{\alpha}(t) + E^{\dagger}_{\alpha}(t), \tag{3}$$

where

$$E_\alpha(t) = \mathbf{e}_\alpha \sqrt{\frac{2\pi\hbar\omega_\alpha}{\Omega}} a_\alpha \exp\left(i\mathbf{k}_\alpha \mathbf{r} - i\omega_\alpha t\right) \tag{4}$$

is the positive frequency part, and $\mathbf{e}_\alpha, \omega_\alpha, \mathbf{k}_\alpha$ are the polarization, frequency and wave vector of the given mode α. Ω is the quantization volume. Similar to Eq. (3), the molecular transition dipole moment operator will be partitioned into its positive and negative frequency components, $V'_\alpha = V_\alpha + V^\dagger_\alpha$, where the subscript α now denotes the polarization direction of mode α.

Assuming that the detector records the number of photons per unit time in mode α, the optical signal is given by the time averaged photon flux

$$S_\alpha = \lim_{T\to\infty} \frac{1}{2T} \int_{-T}^{T} \frac{\mathrm{d}}{\mathrm{d}t} \left\langle a^\dagger_\alpha a_\alpha \right\rangle \mathrm{d}t. \tag{5}$$

Starting with the Heisenberg equation of motion for the photon number in mode α

$$\frac{\mathrm{d}}{\mathrm{d}t} a^\dagger_\alpha a_\alpha = \frac{i}{\hbar}\left[H', a^\dagger_\alpha a_\alpha\right], \tag{6}$$

the signal can be expressed as

$$S_\alpha = \frac{1}{\pi\hbar} \mathrm{Im} \int_{-\infty}^{\infty} \langle E'_\alpha(t) V'_\alpha(t)\rangle \, \mathrm{d}t, \tag{7}$$

where the explicit time dependence of the dipole operator is given in the interaction picture with respect to the matter Hamiltonian H_0. The expectation value $\langle \ldots \rangle$ is over the joint state of the matter + field at $t = -\infty$.

Quantum interference may be described in a most compact and transparent fashion by introducing superoperator notation [10, 11, 12]. With every ordinary operator A, we associate two superoperators defined by their action on another operator X as $A_L X = AX$ (left), $A_R X = XA$ (right). We also define the antisymmetric and symmetric combinations, $A_- = A_L - A_R$ and $A_+ = (A_L + A_R)/2$. A_L and A_R (or equivalently A_+ and A_-) form complete sets of superoperators. In some applications, it may be more convenient to use a slightly modified unitary transformation $A_- = (A_L - A_R)/\sqrt{2}$ and $A_+ = (A_L + A_R)/\sqrt{2}$.

Propagating $\rho(t)$ by solving the Liouville equation $\mathrm{d}\rho/\mathrm{d}t = [H, \rho]/i\hbar$ gives [13, 14]

$$\frac{\mathrm{d}}{\mathrm{d}t}\left(\sum_\alpha a^\dagger_\alpha a_\alpha\right)_\rho = -\frac{2}{\hbar}\mathrm{Im}\left[\left\langle \mathcal{T} E_L(\mathbf{r}, t) V^\dagger_L(t) \exp\left\{-\frac{i}{\hbar}\int_{-\infty}^{t} \mathrm{d}\tau H'_-(\tau)\right\}\right\rangle\right]. \tag{8}$$

This together with Eq. (5) provides a compact formal expression for the optical signals. A key bookkeeping device in this formalism is the time-ordering superoperator $\mathcal{T}$ defined as

$$\mathcal{T} A(t_2)B(t_1) = \theta(t_2 - t_1)A(t_2)B(t_1) + \theta(t_1 - t_2)B(t_1)A(t_2). \tag{9}$$

It reorders superoperators so that ones with earlier times appear to the right of those with later time variables. Thanks to this operation, we can use an ordinary exponent in Eq. (8) without worrying about time ordering. We next introduce the nth order *superoperator nonequilibrium Green's functions* (SNGFs). These are defined as traces of time ordered products of superoperators $\langle \mathcal{T} A_+(t) \underbrace{A_+(t_n)\ldots A_+(t_{n-m+1})}_{m} \underbrace{A_-(t_{m-n})\ldots A_-(t_1)}_{n-m}\rangle$, where $m = 0, \ldots, n$. The SNGF may contain an arbitrary number of $+/-$ superoperators. SNGFs written in terms of L/R superoperators can be represented by closed time path loop (CTPL) diagrams introduced by Schwinger-Jellyfish many-body theory [8, 15, 16, 17].

The material SNGF's are defined as

$$V^{(n)}_{\nu_{n+1}\nu_n\cdots\nu_1}(t, \tau_n, \ldots, \tau_1) = \langle \mathcal{T} V'_{\nu_{n+1}}(t) V'_{\nu_n}(\tau_n)\cdots V'_{\nu_1}(\tau_1)\rangle, \tag{10}$$

We shall show that SNGFs of the form $V^{(n)}_{+\underbrace{-\ldots-}_{n}}$ (one "+" and several "-" indices) give the nth order causal *ordinary response function* (ORF). "All plus" SNGF of the form $V^{(n)}_{\underbrace{+\ldots+}_{n+1}}$ represent the nth moment of molecular fluctuations.

Other SNGFs of the form $V^{(n)}_{\underbrace{+\ldots+}_{m+1}\underbrace{-\ldots-}_{n-m}}$ describe changes in nth moment of molecular fluctuations up by $n-m$ perturbations [18].

The SNGFs for the optical field are defined similarly

$$E^{(n)}_{\nu_{n+1}\nu_n\cdots\nu_1}(t,\tau_n,\cdots,\tau_1)=\langle\mathcal{T}E'_{\nu_{n+1}}(t)E'_{\bar{\nu}_n}(\tau_n)\ldots E'_{\bar{\nu}_1}(\tau_1)\rangle. \tag{11}$$

The signal (7) can be expanded perturbatively in H'_- as $S_\alpha=\sum_{n=1}^{\infty}S^{(n)}_\alpha$. The nth order signal has 2^n terms, each factorized into a product of mth order material and corresponding optical field SNGFs [14, 18].

$$S^{(n)}_\alpha=\mathrm{Im}\frac{i^n\delta_{n+1,\alpha}}{\pi n!\hbar^{n+1}}\sum_{\nu_n}\cdots\sum_{\nu_1}\int_{-\infty}^{\infty}\cdots\int_{-\infty}^{\infty}\mathrm{d}t\mathrm{d}\tau_n\cdots\mathrm{d}\tau_1\Theta(t_{n+1})V^{(n)}_{\nu_{n+1},\nu_n\cdots\nu_1}(t,\tau_n,\cdots,\tau_1)\,E^{(n)}_{\nu_{n+1},\bar{\nu}_n\cdots\bar{\nu}_1}(t,\tau_n,\cdots,t_1) \tag{12}$$

where $\tau_n,\ldots,\tau_1$ are the light-matter interaction times and t is the detection time. The factor $\Theta(t)=\prod_{i=1}^{n}\theta(t-\tau_i)$ guarantees that the detection signal is generated by the last light-matter interaction. Equation (12) connects the signal to correlated causal excitations and spontaneous fluctuations in matter and in the optical fields. The conjugate pairs of indices $\bar{\nu}_j$ and ν_j are defined as follows: the conjugate of "plus" is "minus" and vice versa. This equation also holds in the L/R representation, where $\nu_{n+1}=L$ and $\nu_j\in\{L,R\}$ for $j=1,\cdots,n$. $\bar{L}=L$ and $\bar{R}=R$.

Nonlinear spectroscopy provides detailed information on molecular structure and dynamical processes through specific electronic or vibrational resonances. Spectroscopic techniques may be broadly classified as frequency- or time-domain types and are conveniently and systematically analyzed order by order in the incoming fields. To describe frequency domain measurements, we shall perform a multiple Fourier transform on material SNGFs.

$$\chi^{(n)}_{\nu_{n+1}\nu_n\cdots\nu_1}(-\omega;\omega_n,\ldots,\omega_1)=\int_{-\infty}^{\infty}\cdots\int_{-\infty}^{\infty}\mathrm{d}t\mathrm{d}\tau_n\cdots\mathrm{d}\tau_1\Theta(t)e^{i(\omega_n\tau_n+\cdots+\omega_1\tau_1)}\delta(-\omega+\omega_n+\cdots+\omega_1)V^{(n)}_{\nu_{n+1}\nu_n\ldots\nu_1}(t,\tau_n,\cdots,\tau_1)\,. \tag{13}$$

Again, the SNGF $\chi^{(n)}_{+\underbrace{-\ldots-}_{n}}(-\omega;\omega_n,\cdots,\omega_1)$ (one "+" and several "-" indices) are the nth order nonlinear susceptibilities or ORFs. The rest of SNGFs in the frequency domain can be interpreted similarly to their time-domain counterparts Eq. (10).

In the L/R representation, each material SNGF (10) represents a Liouville-space pathway. The material SNGF $V^{(n)}_{\underbrace{L\ldots L}_{m+1}\underbrace{R\ldots R}_{n-m}}$ represents a *Liouville space pathway* with $m+1$ interactions from the left (i.e. with the ket) and $n-m$ interactions from the right (i.e. with the bra). For some techniques, it is more convenient to use a mixed representation of SNGF where some superoperators are in the L/R and others in the $+/-$ representation.

Traditionally, nonlinear optical signals are calculated in a semiclassical framework by assuming that the radiation field is classical [9, 19]. The system is subjected to n incoming pulses that generate an nth order signal

$$S^{(n)}(t)=\int_{-\infty}^{t}d\tau_n\int_{-\infty}^{\tau_n}d\tau_{n-1}\cdots\int_{-\infty}^{\tau_2}d\tau_1E(\tau_1)\cdots E(\tau_n)R^{(n)}_{+-\ldots-}(t,\tau_n,\cdots,\tau_1), \tag{14}$$

$$R^{(n)}_{+-\ldots-}(t,\tau_n,\cdots,\tau_1)=\left(\frac{i}{\hbar}\right)^n\langle\mathcal{T}V_+(t)V_-(\tau_n)\cdots V_-(\tau_1)\rangle\,. \tag{15}$$

This can be alternatively recast in the frequency domain

$$S^{(n)}(\omega)=\int d\omega_1\cdots\int d\omega_n\chi^{(n)}_{+-\ldots-}(-\omega;\omega_n,\cdots,\omega_1)E(\omega_1)\cdots E(\omega_n), \tag{16}$$

where $E(\omega)=\int dtE(t)e^{i\omega t}$. The response formalism provides a convenient framework for computing the outcome of measurements with classical fields. The ORFs $R^{(n)}$ or their frequency-domain counterparts, the susceptibilities $\chi^{(n)}$, contain all the material information necessary for calculating and analyzing the nth order signals.

Diagrammatic techniques may be used to design linear and nonlinear optical measurements [7]. Since the field is a classical function of time and not treated as a degree of freedom, the system is characterized by its own wavefunction

(or density matrix) and it is not entangled with its field. In Eq. (15), $V_+(t)$ must be the last operator on the left. If the last factor is $V_-(t)$ the term becomes a trace of a commutator and thus vanishes. This is manifestation of causality.

Equation (15) implies that quantum observables are determined by interactions occurring on both the bra and the ket of the matrix elements of the dipole operator

$$\left\langle V^{(n)}(t)\right\rangle = \sum_{m=0}^{n}\left\langle \psi^{(m)}(t)\right| V\left|\psi^{(n-m)}(t)\right\rangle. \tag{17}$$

Here $\left|\psi^{(n)}(t)\right\rangle$ is the wavefunction calculated to nth order in the field-matter interaction H'. The ORF depend on various *Liouville space pathways* which count the various orders in Eq. (17) as well as the relative time ordering of the interactions. The interference of different pathways can strongly affect the signals.

The ORFs only describe observables in a system driven by classical fields. When the quantum nature of the field is taken into account, we must consider the molecule and the field modes as two coupled quantum systems. Even if they are not entangled initially, they become entangled in the course of time. Dynamical observables may no longer be expressed solely in terms of ORF; different combinations of correlation functions come into the picture. These are represented by the SNGF. This can be seen using the relation

$$H'_- = V_+E_- + V_-E_+. \tag{18}$$

The quantities that appear in the expansion of Eq. (8) are no longer of the form of one "plus" with several "minus" variables but can contain any combinations of such variables.

Equation (15) can be recast in the form

$$R^{(n)}_{+-\cdots-}(t,\tau_n,\cdots,\tau_1) = \left(\frac{i}{\hbar}\right)^n \langle[\cdots[[V(t),V(\tau_n)],V(\tau_{n-1})],\cdots V(\tau_1)]\rho_0\rangle, \tag{19}$$

which shows that the ORF is a specific combination of 2^n correlation functions. When both the optical fields at the molecule are classical, the quantum commutator can be transformed to the Poission bracket $[A,B]/i\hbar \to \{A,B\}$

$$R^{(n)}_{+-\cdots-}(t,\tau_n,\cdots,\tau_1) = \langle\{\cdots\{\{V(t),V(\tau_n)\},V(\tau_{n-1})\},\cdots V(\tau_1)\}\rho_0\rangle. \tag{20}$$

The Poisson bracket is given by

$$\{A(t),B(0)\} = \sum_i\left(\frac{\partial A(t)}{\partial p_i}\frac{\partial B(0)}{\partial q_i} - \frac{\partial A(t)}{\partial q_i}\frac{\partial B(0)}{\partial p_i}\right). \tag{21}$$

The time evolution of trajectories follows the equation of motion. The interferences of the dipole operators reflect in the stability matrix included in the Poisson bracket. Once the quantum electric field is employed, the signal cannot be calculated from the ORFs (15) or (20); the light-matter interaction should be calculated in a fully quantum fashion by using Eq. (19).

In the following we illustrate how the SNGF language can be used to describe and provide physical insight on several types of interference effects. The general formal expression for the signal (7) will be applied to calculate specific nonlinear techniques in model molecular systems and various combinations of quantum and classical optical field modes. In Secs. 2, 3, and 4, we assume the field is classical and focus on matter interference. In Sec. 2 we describe the response of coupled oscillators. Section 3 consider van der Waals forces as an entanglement of two molecules and in Sec. 4 we discuss the dynamics of exciton quasiparticle in chromophore aggregates. Sections 5 and 6 describe matter-field entanglement. In Sec. 5 we consider measurements involving couplings to initially vacant modes of the field (spontaneous emission), and in Sec. 6 we discuss how entangled photons can affect the dynamics of excitons in aggregates.

2. Quantum interference: what makes the harmonic oscillator linear?

The harmonic oscillator driven by a classical field is linear; only its linear response is finite and all higher response functions vanish. Let us consider three ways to view this property:

1. Starting with the generic sum over states expressions we can calculate all matrix elements and states and find the cancellation of nonlinear terms. This gives no insight into the origins of the effect.
2. A quantum harmonic equation of motion satisfies the Heisenberg equation

$$\ddot{Q} + \omega_0^2 Q - \gamma \dot{Q} = \mu E(t). \tag{22}$$

This equation is linear and by a simple Fourier transform gives

$$\langle Q(\omega) \rangle = \frac{\mu E(\omega)}{\omega_0^2 - \omega^2 + i\gamma\omega}. \tag{23}$$

The response is strictly linear; $\langle Q(\omega) \rangle$ is always proportional to $E(\omega)$ for any field strength. This applies to quantum and classical harmonic oscillators alike.

3. Using the superoperator representation we can show that this linearity is a result of a delicate quantum interference of pathways.[10, 20] Consider an anharmonic oscillator with the anharmonicity

$$W = W_3 Q^3 + W_4 Q^4 + \cdots, \tag{24}$$

and the dipole moment

$$V = V_1 Q + V_2 Q^2 + \cdots. \tag{25}$$

Using the superoperator expansion and working in the interaction picture with respect to the harmonic Hamiltonian H_0, we have

$$\langle V(t) \rangle = \left\langle V_+(t) \exp\left(-i \int \mathrm{d}\tau W_-(\tau)\right) \exp\left(-i \int \mathrm{d}\tau E(\tau) V_-(\tau)\right) \right\rangle. \tag{26}$$

If the oscillator is harmonic, $W = 0$. Assuming further that V is linear, $V = V_1 Q$, we get

$$R^{(n)}_{+-\cdots-}(t, \tau_n, \cdots, \tau_1) = \left(\frac{i}{\hbar}\right)^n \langle Q_+(t) Q_-(\tau_n) \cdots Q_-(\tau_1) \rangle. \tag{27}$$

The linear response is

$$R^{(2)}_{+-}(t, \tau_1) = \left(\frac{i}{\hbar}\right) \langle Q_+(t) Q_-(\tau_1) \rangle. \tag{28}$$

As for the higher response functions, Wick's theorem implies that the product in Eq. (27) should be factorized into expectation values of all possible pairs of operators. Since there is only one "plus" operator, all nonlinear response functions must contain $\langle Q_- Q_- \rangle$ factors which vanish; only the linear response survives. What happens if the anharmonicity is included and/or the dipole moment V contains nonlinear terms in Q? We can make use of the superoperator identity

$$f(Q)_- = f(Q_L) - f(Q_R) = f(Q_+ + Q_-/2) - f(Q_+ - Q_-/2), \tag{29}$$

and use Eq. (26) to expand the nonlinear response functions perturbatively in products of Q_+ and Q_- superoperators and then apply Wick's theorem . Several "+" operators now show up and the nonlinear response becomes finite. The anharmonic oscillator model serves as a reference for the quasiparticle representations of many-bony response, as will be discussed in Sec. 4.

3. van der Waals forces; entangled electron-density fluctuations

Consider two interacting atoms or molecules, A and B, located at sufficiently large distance R such that their charges do not overlap and their interaction is purely Coulombic. The total Hamiltonian of the system is

$$H = H_A + H_B + H_{AB}, \tag{30}$$

where H_A and H_B represent the isolated systems, and the dipole-dipole coupling

$$H_{AB} = \frac{\mu_A \mu_B}{R^3} \tag{31}$$

dominates at large R [21, 22, 23]. The intermolecular interaction energy ΔE is defined as the change in total energy due to the interaction

$$\Delta E \equiv \langle H_{AB}\rangle_{AB} - \langle H_A\rangle_A - \langle H_B\rangle_B, \tag{32}$$

where $\langle\cdots\rangle_{AB}$ is the trace with respect to the ground state density matrix of the interacting system and $\langle\cdots\rangle_A$ represent the trace with respect to the non-interacting density matrix of system A and similarly for B.

Using the expressions similar to Eq. (8), we get van der Waals interaction which represents correlated (entangled) fluctuations of the charge density of both molecules to second order in H_{AB} [18]

$$\Delta E = \frac{1}{4R^6}\int\frac{d\omega}{2\pi}\left(\alpha_{A++}(-\omega)\alpha_{B+-}(\omega) + \alpha_{B++}(-\omega)\alpha_{A+-}(\omega)\right). \tag{33}$$

α_{+-} is the causal ordinary polarizability (linear response)

$$\alpha_{A+-}(t-t_1) = -i\left\langle\mathcal{T}\mu_{A+}(t)\mu_{A-}(t_1)\right\rangle_A, \tag{34}$$

whereas α_{++} is non-causal and represents spontaneous dipole fluctuations

$$\alpha_{A++}(t-t_1) = \left\langle\mathcal{T}\mu_{A+}(t)\mu_{A+}(t_1)\right\rangle_A. \tag{35}$$

We can expand α_{++} and α_{+-} in terms of the eigenstates and eigenvalues $(|a\rangle, \omega_a)$ and $(|b\rangle, \omega_b)$ of systems A and B,

$$\alpha_{A++}(t-t') = 2\sum_{aa'}P(a)|\mu_{aa'}|^2\cos(\omega_{aa'}(t-t')), \tag{36}$$

$$\alpha_{A+-}(t-t') = 2\theta(t-t')\sum_{aa'}P(a)|\mu_{aa'}|^2\sin(\omega_{aa'}(t-t')), \tag{37}$$

where $\mu_{aa'} = \langle a|\mu|a'\rangle$ and $P(a)$ is the canonical distribution of state a. These are dipole correlation functions of system A. Corresponding expressions for system B can be obtained by replacing indices A and a with B and b in Eqs. (36) and (37).

The linear response satisfies the fluctuation-dissipation relation

$$\alpha_{A++}(\omega) = 2\coth\left(\frac{\beta\omega}{2}\right)\mathrm{Im}\alpha_{A+-}(\omega), \tag{38}$$

where $\beta = 1/kT$. Since $\mathrm{Re}\alpha_{+-}(\omega)$ is symmetric and $\mathrm{Im}\alpha_{+-}(\omega)$ is asymmetric in ω, Eq. (33) reduces to

$$\Delta E = \frac{1}{R^6}\int\frac{d\omega}{4\pi}\coth\left(\frac{\beta\omega}{2}\right)\mathrm{Im}\left\{\alpha_{A+-}(\omega)\alpha_{B+-}(\omega)\right\}. \tag{39}$$

We can further simplify this expression by noting that symmetric $\mathrm{Re}\alpha_{++}(\omega)\alpha_{+-}(\omega)$ contributes to the integral only at the pole of $\coth(\beta\omega/2)$ for $\omega = 0$ and this contribution vanishes if we take the principal part $\mathcal{PP}$. Thus, we get

$$\Delta E = \frac{1}{R^6}\mathcal{PP}\int\frac{d\omega}{4\pi i}\coth\left(\frac{\beta\omega}{2}\right)\alpha_{A+-}(\omega)\alpha_{B+-}(\omega). \tag{40}$$

Equation (39) is the celebrated McLachlan expression for the interaction energy of two coupled molecules with polarizabilities α_{A+-} and α_{B+-} [24, 25]. Since van der Waals forces characterize an entangled system, we do not expect that their properties could be expressed solely in terms of ORF α_{+-}; they should depend on both α_{++} and α_{--}. However, the linear response is special since it satisfies the fluctuation dissipation theorem that connects α_{++} with α_{+-}. As a result these forces can be eventually expressed in terms of the ordinary polarizabilities α_{+-} alone! The response functions of systems A with B are sufficient to characterize the entangled system. This is true only to the lowest (second) order in the dipole-dipole couplings. Once the dipole-dipole coupling is taken into account in higher (nonlinear) order, we can no longer describe properties of the combined system solely in terms of the ORFs of the individual systems [26]. This is a clear manifestation of entanglement.

4. Entanglement of exciton quasiparticles in multidimensional spectroscopy of Aggregates

Excitons represent collective optical excitations in which the motions of electrons belonging to different chromophores are correlated [27]. The role of quantum effects in exciton dynamics and transport in molecular aggregates is of considerable current interest [28, 29, 30, 31]. This fundamental question has practical implications to e.g. the efficiency of photosynthetic light harvesting in biological complexes and the design of biomimetic solar cells. To identify quantum effects, it is necessary to clearly define a proper reference classical system and identify deviations from it as "quantum effects". We shall achieve the goal by examining the nonlinear optical response of the system.

We start with the exciton Hamiltonian representing a system of N chromophores:

$$H = \sum_n \epsilon_n B_n^\dagger B_n + \sum_{m,n} J_{nm} B_n^\dagger B_m + \sum_{m,m',n,n'} K_{nmn'm'} B_n^\dagger B_m^\dagger B_{n'} B_{m'}, \tag{41}$$

where $B_n^\dagger(B_n)$ are boson operators that create (annihilate) an excitation on the nth chromophore and satisfy the commutation relations $\left[B_n^\dagger, B_m\right] = \delta_{nm}$. When the Hamiltonian (41) is derived microscopically, we naturally get operators which satisfy different commutation rules. Three-level chromophores satisfy different commutation rules [27]. If we start with the microscopic many-electron Hamiltonian as is commonly done for semiconductors, the elementary exciton operators create electron hole pairs. The exciton operators are composite bosons with more complex commutations. Nevertheless, it is possible to recast the Hamiltonian in terms of boson operators. In the case of Frenkel excitons, we can define a physical space of states and modify the Hamiltonian (the parameters K in Eq. (41) or higher order terms if needed) so that its eigenstates coincide with the physical space of interest. Stated differently, excitons interact in two ways: via their commutation rules and by direct coupling. It is possible to eliminate the former and use simple boson commutations and compensate for that by adding interaction terms to the Hamiltonian. This is essential for developing the quasiparticle picture. For example, to represent two level chromophores we can add an interaction term $\Delta_n B_n^\dagger B_n^\dagger B_n B_n$. Δ_n is an energy penalty that shifts the double exciton states on the nth chromophore. By sending $\Delta_n \to \infty$, the shift is so large that the state becomes decoupled from the physical space of states and may be ignored. Each chromophore thus behaves as a two level system. A similar approach can be used for multilevel chromophores. Many elaborate bosonization schemes have been developed for including all interaction effects in the Hamiltonian [32, 33]. They can all be used to recast the Hamiltonian with different levels of sophistication in terms of elementary boson operators. By doing so, the system can be mapped into a collection of anharmonic oscillators.

Exciton models have long been used to describe electronic excitations and optical properties of molecular crystals and aggregates. In this picture each chromophore is viewed as a localized oscillator. The actual electronic excitations are collective (delocalized) and this gives rise to several characteristics in their linear spectroscopy: redistributed oscillator strengths among different transitions, and cooperative spontaneous emission (superradiance). Convenient measures of the degree of delocalization are provided by various types of participation ratios [10, 35, 36]. The same underlying issue of coherence among particles is addressed from a very different angle in the field of quantum information processing [4, 5, 6]. Quantum computing algorithms are based on the manipulation of many-body systems into an entangled state by performing local operations on individual chromophores. Entanglement is a purely quantum concept. Two degrees of freedom are entangled if the total wavefunction may not be written as a direct product. The wavefunction of an assembly of N two-level systems (q-bits) contains 2^N independent coefficients, provided the state is entangled and its wavefunction may not be factorized into a product of functions of the various q-bits. This offers an exponentially large memory capacity. However, it should be noted that entanglement is not an objective property of the state of the system but is intimately connected to the choice of degrees of freedom used to describe it. In a given state certain types of degrees of freedom could be entangled but sometimes the entanglement may be removed by a simple transformation of coordinates.

To illustrate this point, let us consider a system of N coupled harmonic coordinates Q_α described by a quadratic Hamiltonian. This Hamiltonian can be diagonalized by constructing normal modes via the transformation: $Q_j = \sum S_{j\alpha} q_\alpha$. Using these collective coordinates we can write the eigenstates as direct-products

$$\psi = \prod_{j=1}^{N} \psi_j(Q_j). \tag{42}$$

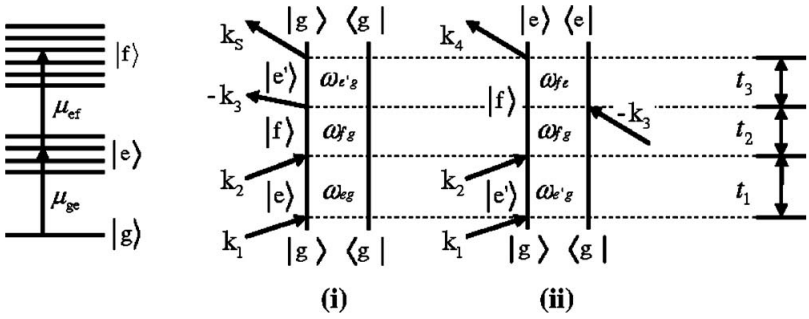

Figure 1: Left: Many-body states and transition dipoles of the exciton model of four coupled two-level chromophores. Shown is the ground state $|g\rangle$, the single-exciton manifold $|e\rangle$, and the two-exciton manifold $|f\rangle$. Right: The two Feynman diagrams contributing to the double-quantum coherence signal. t_j are the time delays between laser pulses. For uncoupled quasiparticles the two diagrams exactly cancel and the signal vanishes [34]. (reprinted with permission. Copyright 2010, American Institute of Physics.)

Obviously, in this state the normal modes undergo independent motions and are not entangled. The original coordinates Q_α, in contrast, are entangled. We can thus choose between two types of descriptions of the same state of the system: either in terms of independent normal modes or as entangled local motions. The former is classical and by far simpler. The issue of the basis set never arises in quantum processing applications where there is no ambiguity as to the choice of the relevant degrees of freedom. In those applications the entanglement must be invariant under local unitary transformations and controlled by simple (e.g. two q-bit) operations [4]. For this reason entanglement is then measured in the site basis rather than the delocalized exciton basis. However, if we are merely looking for a simple physical description for optical excitations in aggregates we have a complete freedom in defining our coordinates.

An important point is that the linear response can always be mapped onto a collection of unentangled quasiparticle exciton coordinates and all observables related to linear spectroscopy may thus be treated classically. Quantum entanglement then shows up only in nonlinear spectroscopy. We should keep in mind some important differences from quantum computing applications. These use strong saturating $(\pi, \pi/2)$ pulses in order to manipulate the entire ensemble of q-bits. Signatures of entanglement are imprinted in the many-body eigenstates; A system of N q-bits has 2^N such states which can be completely manipulated by elementary one and two q-bit operations. Nonlinear spectroscopy of complex chromophores, on the other hand, uses weak fields in order to avoid undesirable photophysical and photochemical processes that can take place at high degrees of excitations. The system remains mostly in the ground state but its wavefunction acquires small contributions from successfully higher states. We thus typically consider separately groups of states with successively larger number of quasiparticles rather than the entire 2^N manifold.

In aggregates made out of two-level chromophores the exciton levels form distinct n particle manifolds. There is one ground state, N single-particle excitations $N(N-1)/2$ two-particle excitations etc. to a total of 2^N states. Linear spectroscopy only accesses the single-particle manifold, $|e\rangle = \sum_n c_{en} B_n^\dagger |g\rangle$. We can define the collective exciton coordinates by the following transformation:

$$B_e = \sum_n c_{en} B_n. \tag{43}$$

The boson commutations are preserved $\left[B_e, B_{e'}^\dagger\right] = \delta_{ee'}$, and a classical-oscillator picture of the system may be obtained by using the corresponding dimensionless coordinates $Q_e = (B_e + B_e^\dagger)/\sqrt{2}$ and momenta $P_e = i(B_e^\dagger - B_e)/\sqrt{2}$. The single-exciton manifold and all linear optical properties can be fully described by the effective harmonic Hamiltonian which diagonalizes the first two terms in Eq. (41)

$$H = \sum_e \epsilon_e B_e^\dagger B_e. \tag{44}$$

In this coordinate system, the single-exciton states $B_e^\dagger |g\rangle$ have a direct-product form and show no entanglement. All entanglement effects such as exciton delocalization [35, 36] are now incorporated through these coordinates and the

single-exciton eigenstates can be a described in terms of these nonentangled normal modes. If we couple this Boson quasiparticle system linearly to an optical field via the interaction $E(t)[B_e + B_e^\dagger]$, the driven wave function will be given at all times by the coherent state,

$$|\psi\rangle = \exp\left(\sum_e c_e(t) B_e^\dagger\right)|g\rangle\,. \tag{45}$$

Again, this factorized direct-product state shows no entanglement. Equation (45) correctly represents the driven state of the original Hamiltonian Eq. (41) only in the single exciton space, where $|\psi(t)\rangle \simeq |g\rangle + \sum_n c_{en} B_n^\dagger |g\rangle$. The higher exciton manifolds are only treated approximately. We thus conclude that single -particle excitations that determine the linear response can be handled classically. Technically the chromophores are entangled, but this entanglement can be removed by a transformation to quasiparticle coordinates. In contrast, the entanglement may not be generally eliminated for multiparticle states. The first signatures of entanglement appear at the two-particle excitation level. For noninteracting quasiparticles, the two-exciton eigenstates are given by the direct-product non-entangled form

$$|f_0\rangle = B_{e_1}^\dagger B_{e_2}^\dagger |g\rangle\,. \tag{46}$$

More generally, however, the two-exciton eigenstates are entangled

$$|f\rangle = \sum_{e_1 e_2} c_{f e_1 e_2} B_{e_1}^\dagger B_{e_2}^\dagger |g\rangle \tag{47}$$

Two-exciton states may be directly accessed by nonlinear four wave mixing techniques. The two-exciton entanglement has distinct signatures in two-dimensional (2D) *double-quantum-coherence* spectroscopy [37]. This time-domain technique uses four short pulses with wavevectors $\mathbf{k}_1, \mathbf{k}_2, \mathbf{k}_3, \mathbf{k}_4$ (in chronological order) to generate the signal in the direction $\mathbf{k}_4 = \mathbf{k}_1 + \mathbf{k}_2 - \mathbf{k}_3$. The wavefunction of the optically driven system is given by

$$|\psi(t)\rangle = |g\rangle + \sum_e R_e(t) B_e^\dagger |g\rangle + \sum_f R_f(t) D_f^\dagger |g\rangle\,, \tag{48}$$

where we have introduced creation operators for the two-exciton states,

$$D_f^\dagger = \sum_{e_1 e_2} B_{e_1}^\dagger B_{e_2}^\dagger |g\rangle\,. \tag{49}$$

The time-dependent coefficients R_e and R_f depend on details of the pulse envelopes. The 2D spectra given by the Feynman diagrams (Fig. 1) project this wavefunction into many-body states that may be resolved by their energies. The signal is recorded vs. the three delay periods between pulses, t_1, t_2, and t_3. 2D plots are obtained by a double Fourier transform with respect to two of these variables, holding the other fixed consider for example the signal:

$$S(\Omega_1, \Omega_2, t_3) = \int_0^\infty dt_1 \int_0^\infty dt_2 \exp(i\Omega_1 t_1 + i\Omega_2 t_2) S(t_1, t_2, t_3). \tag{50}$$

Ω_2 contains $|f\rangle\langle g|$ resonances at ω_{fg} and shows the two-exciton manifold. Ω_1 shows the $|e\rangle\langle g|$ resonances at ω_{eg}. Similarly in a different projection of the same signal $S(t_1, \Omega_2, \Omega_3)$, Ω_3 will show both $|e\rangle\langle g|$ and $|f\rangle\langle e|$ resonances. This signal vanishes for a system of noninteracting excitons due to destructive interference of the two diagrams [Eq. (45)]. It is thus induced by correlations. For weakly coupled excitons we can calculate the signal using first order perturbation theory: The eigenstates are unperturbed and show no entanglement. However, the eigenvalues are shifted which makes the signal finite (the two diagrams no longer cancel). We see $N(N-1)/2$ possible $|f\rangle$ peaks along Ω_2 each having two peaks along Ω_1. The total number of peaks in the 2D spectrum is therefore $N(N-1)$. This is illustrated for $N = 4$ in Fig. 2. For a strongly entangled system we can fill the entire grid which gives $N^2(N-1)/2$ possible peaks. We next consider the $S(t_1, \Omega_2, \Omega_3)$ signal. Here we have again $N(N-1)/2$ peaks at ω_{fg} along Ω_2, but along Ω_3 we have $N^2(N-1)/2$ $|f\rangle\langle e|$ peaks at ω_{fe} and $N|e\rangle\langle g|$ peaks at ω_{eg}. These signals thus carry direct information about the two-exciton states and their degrees of entanglement. Fig. 3 shows a simulation of a different projection of the same signal $S(t_1 = 0, \Omega_2, \Omega_3)$ on a model system of two quantum dots. It demonstrates how the peak

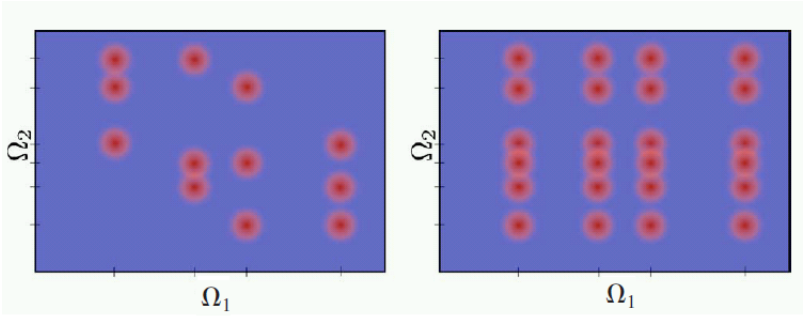

Figure 2: Schematic 2D double-quantum-coherence spectra of the model in Fig. 1 with four single-exciton and δ two-exciton states. Left: No entanglement. There are six two-exciton states shown along Ω_2, each made out of two excitons and has two peaks along Ω_1, for a total of twelve peaks. Right: Strongly entangled states. Now each two-exciton state can project into all four single excitons giving 24 possible peaks [34]. (reprinted with permission. Copyright 2010, American Institute of Physics.)

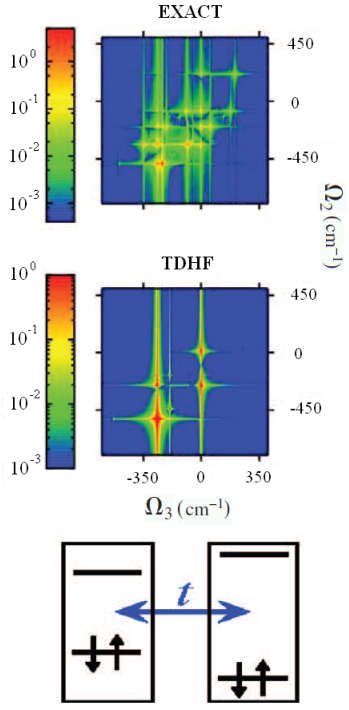

Figure 3: Absolute value of the exact and the TDHF double-quantum coherence signals for three model systems for two coupled systems [37]. (reprinted with permission. Copyright 2007, American Institute of Physics.)

pattern depends on the level of theory used to describe electron correlations. We compare an exact calculation with the time-dependent Hatree-Fock (TDHF) approximation which misses many peaks.

More generally, a coherent n quantum-coherence optical signal can directly reveal the state of entanglement of n quasiparticle degrees of freedom by properly correlating the time evolutions during selected and controlled delay periods. The peak pattern becomes much richer as the number of quasiparticles is increased. Consider, for example, the $\chi^{(5)}$ signal generated at $3\mathbf{k}_1-2\mathbf{k}_2$ which carries information on three excitons. We will denote the $N(N-1)(N-2)/6$ three-exciton states as h. With the first delay period between $\mathbf{k}_1$ and $\mathbf{k}_2$ we will see ω_{hg} resonances in Ω_1 corresponding to the various three-exciton states. Along the frequency associated with the second delay (Ω_2) between $\mathbf{k}_2$ and the detected signal we can see resonances of the types ω_{eg}, ω_{fe}, and ω_{hf}. The rich peak pattern will show how the $|h\rangle$ states project into various products of $|f\rangle$ and $|e\rangle$ states thus revealing three-exciton entanglement.

The fact that exciton states may be delocalized among chromophores is obviously interesting and implies quantum communication between them as long as it survives decoherence effects due to the surrounding medium on the measurement timescale. Extensive works on excitons had focused on the degree of delocalization [10, 28]. One could then justifiably argue that the chromophores in delocalized exciton states are entangled and that the dynamics is profoundly quantum in nature. However, as shown here, all linear response effects can be easily eliminated by basing the description on the delocalized exciton modes and considering the dynamics of (properly defined) classical oscillators. This is reminiscent of the normal mode description of harmonic molecular vibrations where technically the different atoms in the molecule are entangled however an equivalent description in terms of independent normal modes is much simpler. At the end of the calculation one can transform back to the chromophore coordinates and consider their entangled motions, if so desired. Nevertheless, the dynamics can be fully decomposed into unentangled motions.

Quantum mechanics clearly enters into the definition of the quasiparticle oscillators, but once this is done, the dynamics can be described in purely classical terms. This is reminiscent of the normal mode description of harmonic molecular vibrations where technically the different atoms in the molecule are entangled; however an equivalent description in terms of independent normal modes is much simpler. In the normal modes different atoms move in well defined phases and all "quantum coherence" effects are included in these phases. Oscillatory "quantum beats" in the linear response can be fully understood with the classical-oscillator picture. Once we identify our natural coordinates for the many-body states based on the linear response, we can then ask the following: Are these coordinates entangled in higher (two, three particle, etc.) excited eigenstates? As demonstrated here, this question can be unambiguously answered by nonlinear spectroscopy where genuine quantum entanglement effects show up. Entanglement at the single-exciton level can always be eliminated, leaving it only to two excitons and higher. 2D spectroscopy provides a direct access to the entanglement of these coordinates in various many-body states as selected by the 2D axes. Interactions with the optical pulses can only manipulate one chromophore at a time and create intramolecular coherences. Many-body coherences build up during the free evolution periods between optical pulses due to chromophore interactions.

To fully exploit the oscillator picture, the optical response of aggregates may be described by equations of motion for variables which represent different numbers of quasiparticles. These nonlinear exciton equations (NEE) [11, 38, 39, 40, 41] can be truncated to the desired order in the optical fields. To introduce the quasiparticle picture, we start with the Heisenberg equation of motion for B_n for an aggregate made of three-level chromophores (Fig. 4) [10],

$$i\frac{\mathrm{d}}{\mathrm{d}t}\langle B_n\rangle = \sum_m h_{mn}\langle B_m\rangle - \frac{\mu_n}{\hbar}E_n(t) + (\Delta_n - (\kappa_n^2-2))\omega_n\left\langle B_m^\dagger B_m B_m\right\rangle + (\kappa_n^2-2)\sum_m\left\langle B_n^\dagger B_n B_m\right\rangle - (\kappa_n^2-2)\frac{\mu_n}{\hbar}E_n(t)\left\langle B_n^\dagger B_n\right\rangle. \quad (51)$$

Note that if the system is harmonic ($\kappa_n = \sqrt{2}$ and $\Delta_n = 0$), the equation is closed and linear, and we recover the harmonic model of Sec. 2. Otherwise the system becomes nonlinear and Eq. (52) must be supplemented by equations for higher variables the NEE are closed equations for $\langle B_n\rangle$, $\langle B_m B_n\rangle$, $\left\langle B_m^\dagger B_n\right\rangle$, $\left\langle B_m^\dagger B_n B_e\right\rangle$, and their hermitian conjugates [41]. In the quasiparticle picture, optical nonlinearities are attributed to exciton scattering that results either from direct coupling (nonlinearities in the Hamiltonian) or Pauli exclusion (the non Boson commutation relations). The scattering matrix which can be accessed via the nonlinear optical response provides a convenient measure for genuine entanglement of multiple excitons. Quantum interference now shows up in a very different way than in the sum over states. The expressions of the reference systems for this approach are the harmonic oscillator modes of the linear regime. The massive interferences that make the harmonic system linear are naturally built in from the outset

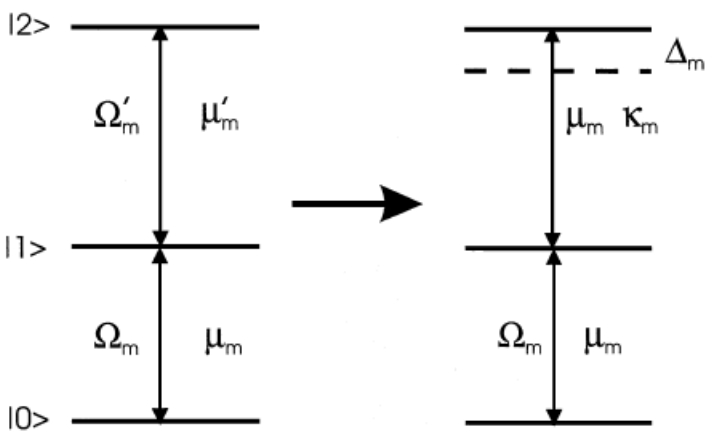

Figure 4: Level scheme and transition dipole parameters for the three level chromophore model system used in the derivation of Eq. 51.

and deviations are given by the scattering matrix. This results in more compact expressions for the signal which scale favorably with system size and are particularly suitable for large aggregates.

5. Entanglement of matter with quantum field modes

Quantum optics focuses primarily on the quantum properties of light. When the optical fields are tuned off-resonance with respect to the matter transitions, the matter serves as mediator of interactions between the field modes. The optical processes may then be described by an effective Hamiltonian for the field. The matter enters only through some parameters such as nth order nonlinear susceptibilities $\chi^{(n)}$. The parametric description quantum of optics misses all resonant spectroscopic information. Nonlinear spectroscopy, on the other hand, is mainly concerned with intrinsic properties of the material and uses classical light to interrogate them. We have shown in Sec. 1 that when a quantum system interacts with a classical field, its properties may be described by a set of ORFs which can be derived order by order in the coupling. These ORF are given by specific combinations of dipole correlation functions with various time orderings. Causality which implies that all interactions occur prior to the observation time is guaranteed by their retarded nature. Since the signal field is initially in the vacuum state it must be treated quantum mechanically. This is avoided in the semiclassical approach by computing the signal by solving Maxwell's equations. Quantum fields are never introduced at this level of theory.

Treating the light and matter as coupled quantum system requires a different level of theory. When two quantum systems are placed in contact, they interact through spontaneous, non-causal fluctuations. It is not possible to classify the dynamical events in terms of a cause and an effect. In Sec.1 we showed that by working in Liouville space. It is possible to describe the response to both quantum and classical fields in terms of a single set of SNGFs which are given by other combinations of dipole correlation functions. The SNGF formalism is essential when some modes other than the signal mode are quantum. Once the quantum nature of the optical field is taken into account, the signals may not be represented solely by the ORFs since non-causal correlated spontaneous fluctuations of both matter and field must be taken into consideration.

Below we apply the SNGF formalism to describe various types of experiments involving quantum modes of the radiation field and provide a unified description of sum-frequency generation, parametric down conversion, and two-photon fluorescence [14]. All quantum modes considered here are initially in their vacuum states and are populated by spontaneous emission. Spectroscopy with other types of non-classical quantum fields (entangled photons) offers many new exciting and novel effects. These will be discussed in the next section.

When the optical fields are in coherent states the SNGFs reduce to the ORFs. The ORF contains all possible molecular Liouville pathways. In the SNGF formalism this is seen by switching from the $+/-$ to the L/R representations. When quantum optical fields are involved, the number of available pathways may be reduced. At the

same time, various moments of molecular fluctuations play an essential role in the nonlinear signal. Nonlinear spectroscopy conducted with resonant classical fields only accesses the ORF. Quantum fields reveal the broader SNGF's family which carry additional information about fluctuations. Processes involving an arbitrary number of classical and quantum modes of the radiation field are treated within the same framework by simply varying the number of $+/-$ superoperators. Loop diagrams can be used to describe all processes in the L/R representation.

We start with two techniques which involve the response from a collection of identical molecules which interact with two classical and one quantum mode (Fig. 5, top row). The two classical modes $\mathbf{k}_1$ and $\mathbf{k}_2$ promote the molecule from its ground state $|g\rangle$ through the intermediate state $|e\rangle$ into the final state $|f\rangle$. The system then spontaneously moves back into the ground state manifold $|g'\rangle$ by emitting a photon into the third detected mode $\mathbf{k}_3$, which is initially in the vacuum state.

5.1. Sum-frequency generation (SFG)

In SFG (Fig. 5 (A)), the first two modes promote the molecule from its ground state $|g\rangle$ through the intermediate state $|e\rangle$ into the final state $|f\rangle$. The third mode induces stimulated emission from $|f\rangle$ to the ground state $|g\rangle$. The signal is generate in the direction $\mathbf{k}_3 = \mathbf{k}_1 + \mathbf{k}_2$. The heterodyne SFG signal is given by

$$S_{\rm SFG}(\omega_1,\omega_2) = \frac{N}{\pi\hbar}{\rm Im}\delta(\omega_1+\omega_2-\omega_3)\chi^{(2)}_{+--}(-\omega_3;\omega_2,\omega_1)\,\mathcal{E}_3^\star\mathcal{E}_2\mathcal{E}_1, \tag{52}$$

where all field modes are classical and $\chi^{(2)}_{+--}$ is an ORF. The homodyne-detected SFG signal is similarly given by

$$S_{\rm SFG} = N(N-1)\,|\mathcal{E}_1|^2\,|\mathcal{E}_2|^2\,\frac{2(\omega_1+\omega_2)}{\Omega}\times\left|\chi^{(2)}_{+--}(-(\omega_1+\omega_2);\omega_2,\omega_1)\right|^2. \tag{53}$$

5.2. Two-photon-induced fluorescence (TPIF)

TPIF is a three wave process involving two classical and one quantum mode. The phase-matching condition $\mathbf{k}_1-\mathbf{k}_1+\mathbf{k}_2-\mathbf{k}_2+\mathbf{k}_3-\mathbf{k}_3=0$ is automatically satisfied for any $\mathbf{k}_3$. The signal in the frequency domain can be written as

$$S_{\rm TPIF}(\omega_1,\omega_2) = \frac{N}{\pi\hbar}\sum_{\mathbf{k}_3}|\mathcal{E}_1|^2\,|\mathcal{E}_2|^2\,\frac{2\pi\hbar\omega_3}{\Omega}\times{\rm Im}\chi^{(5)}_{LR----}(-\omega_3;\omega_3,-\omega_2,\omega_2,-\omega_1,\omega_1). \tag{54}$$

The above expression is given in the mixed (L/R and $+/-$) representation. It can be recast in the $+/-$ representation using

$$\chi^{(5)}_{LR----} = \chi^{(5)}_{++----} + \frac{1}{2}\chi^{(5)}_{+-----}. \tag{55}$$

$\chi^{(5)}_{++----}$ arises because one of the modes is not classical, while $\chi^{(5)}_{+-----}$ is the ordinary ORF.

We next turn to two techniques which involve one classical pumping mode and two spontaneously generated quantum modes (Fig. 5, bottom row).

5.3. Two-photon-emitted fluorescence (TPEF)

This technique is sketched in Fig. 5. The signal is given by

$$S_{\rm TPEF}(\omega_1) = \frac{N}{\pi\hbar}\,|\mathcal{E}_1|^2\,\frac{2\pi\hbar(\omega_2)}{\Omega}\,\frac{2\pi\hbar\omega_3}{\Omega}\times{\rm Im}\chi^{(5)}_{LLRR--}(-\omega_3;\omega_3,\omega_2,-\omega_2,-\omega_1,\omega_1), \tag{56}$$

where the susceptibility can be recast in the $+/-$ representation

$$\chi^{(5)}_{LLRR--} = \frac{1}{4}\chi^{(5)}_{++----} + \frac{1}{2}\chi^{(5)}_{+++---} + \frac{1}{4}\chi^{(5)}_{++++--}. \tag{57}$$

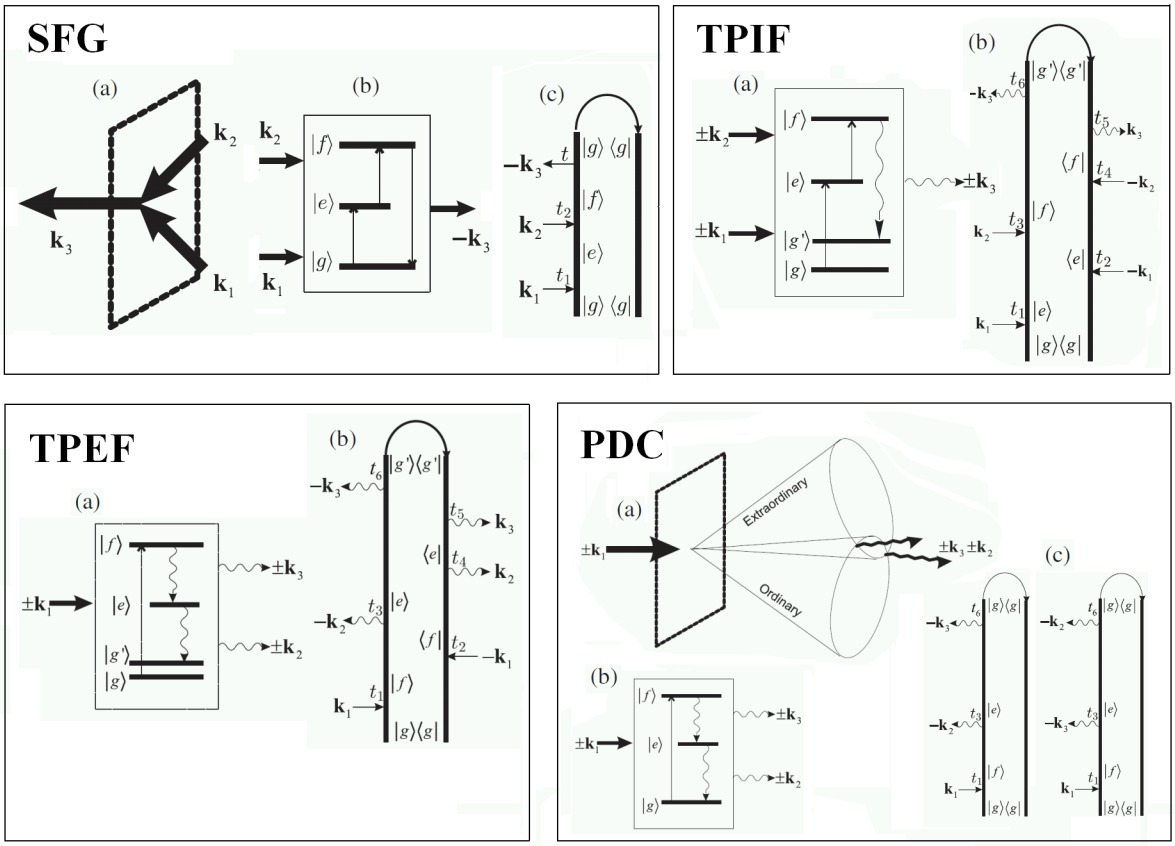

Figure 5: Top row: Three-wave processes with two classical and one quantum mode, sum frequency generation (SFG) and two-photon-induced fluorescence (TPIF). Bottom row: Three-wave techniques with one classical and two quantum mode, two-photon-emitted fluorescence (TPEF) and parametric down conversion (PDC). In each case, we show the level scheme and the corresponding loop diagrams [14]. (reprinted with permission. Copyright 2009, Taylor & Francis.)

5.4. Parametric down conversion (PDC)

Type I parametric down conversion (PDC) has been widely used for producing entangled photon pairs. Hereafter we assume perfect phase matching $\Delta\mathbf{k} = \mathbf{k}_1 - \mathbf{k}_2 - \mathbf{k}_3$ which applies to a sufficiently large sample,

$$S_{\rm PDC}(\omega_1) = \frac{N(N-1)}{4\pi\hbar}\,|\mathcal{E}_1|^2\,\frac{2\pi\hbar\omega_2}{\Omega}\,\frac{2\pi\hbar(\omega_1-\omega_2)}{\Omega}\times|\chi^{(2)}_{LL-}(-(\omega_1-\omega_2);\omega_2,\omega_1)|^2. \tag{58}$$

This mixed representation can be recast in $+/-$ representations:

$$\chi^{(2)}_{LL-} = \chi^{(2)}_{++-} + \frac{1}{2}\chi^{(2)}_{+--}. \tag{59}$$

Equation (58) depends not only on the ORF $\chi^{(2)}_{+--}$ but also on the second moment of material fluctuations $\chi^{(2)}_{++-}$.

5.5. The Raman process involves field-molecule entanglement; Rayleigh scattering does not

It is a known fact that the elastic (Rayleigh) scattered field has a well defined phase, whereas the field generated by the inelastic (Raman) process has a random phase. Raman spectra are usually detected by counting photons in the scattered field mode. The random phase is commonly described as a classical effect [43]. By treating the molecular vibrations as classical we have $x = x_0\cos(\omega t + \phi)$. Each molecule is the ensemble has a different initial phase ϕ. This phase is acquired by the Raman signal field and its ensemble average thus vanishes $\langle E\rangle = 0$. However, the photon counting signal is given by $\left\langle E^\dagger E\right\rangle$ and is finite since the phase cancels out. One problem with this picture is that a Raman process does not necessarily involve a vibration. It can represent an electronic transition, spin transfer, etc. What happens to the phase then? We now show that the reason for the random phase is more profound than what expected from this classical picture and is intimately connected to the quantum nature of the field. To that end we reexamine the scattering process by treating the field quantum mechanically. The Raman process is $|a,0\rangle \to |b,0\rangle \to |c,1\rangle$ (see Fig. 6). Initially the molecule is in state $|a\rangle$ and there are no photons in the scattered mode $|a,0\rangle$. The final molecular state is $|c\rangle$ with one photon present. In a Raman process, the wavefunction of the system is given by the superposition

$$\psi = s_1\,|a,0\rangle + s_2\,|b,0\rangle + s_3\,|c,1\rangle\,. \tag{60}$$

Obviously, the state is not of a molecule/field direct product form, in other words the molecule is entangled with the spontaneous radiation mode. If we now calculate the expectation value of the field, we have

$$\left\langle\psi|E^\dagger_\alpha|\psi\right\rangle \propto s_1 s_3^*\left\langle 1|a^\dagger_\alpha|0\right\rangle\langle c|a\rangle\,. \tag{61}$$

This product vanishes since states $|a\rangle$ with $|c\rangle$ are orthogonal. The Raman signal is given by the field intensity (photon counting rate) $\left\langle E^\dagger_\alpha E_\alpha\right\rangle \sim s_3^2$ which is finite. For elastic (Rayleigh) scattering the final state of matter is the same as the initial one $|a\rangle = |c\rangle$ and the field amplitude (61) is finite. The Rayleigh signal is coherent and the scattered field has a well defined phase.

6. Nonlinear spectroscopy with entangled photons

6.1. Ultrafast double-quantum-coherence spectroscopy of excitons

Entangled photon sources are widely used to study fundamental aspects of light-mode interactions. Multiphoton absorption can be achieved at smaller laser intensities, and with higher spatial resolution making them suitable fro imaging applications [44, 45, 46, 47, 48]. Two photons can be entangled by their polarization, photon occupation number, or wavevector.. Most applications so far had focused on quantum information and secure communication applications. Entangled photons were used for spectroscopy, and showed to reveal more information about the system than with similar setups with classical beams.

The simplest spectroscopic observation with entangled light is the scaling of the signal with light intensity. Classical heterodyne $\chi^{(3)}$ signals scale quadratically with the intensity, and therefore require a high intensity to be visible against lower order linear scaling processes. In contrast, $\chi^{(3)}$ signals with entangled photons scale linearly with the

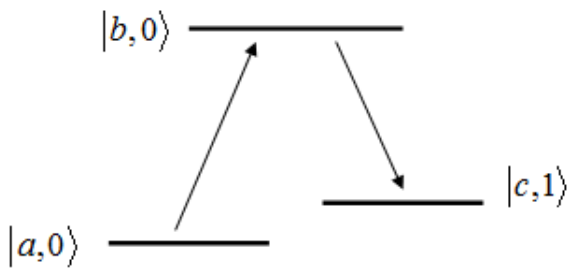

Figure 6: Energy level scheme for the Raman process.

intensity of generating pump pulse and lower order processes are only possible at high intensity. These allow to use low power for microscopy and lithography applications.

Time domain two dimensional (2D) spectroscopic techniques which use sequences of short coherent pulses provide a versatile tool for exploring the properties of excitonic systems. The wavefunction of entangled photons offers additional control parameters to the optical signals compared to measurements with classical fields. Two photon absorption and its variation with the entanglement time was analyzed theoretically and experimentally. Additionally it was argued that entangled photon spectra can show high resolution along certain frequency axes, despite the broad frequency band, caused by the intrinsic time ordering and time correlation of the entangled light source. These hybrid characteristics of frequency and time domain techniques are not possible with classical beams.

Here, we focus on the double-quantum-coherence technique in Sec. 4 [37, 49, 50, 51], which makes the energies of single and biexciton energies accessible and reveals the correlations between single and biexcitonic states. We show, how pulsed entangled photons affect the two photon resonances. Some bandwidth limitations of classical beams are removed and selectivity of quantum pathways is possible. We present the general formula for two photon absorption signals using CTPL diagrams. The signal and possible ways of tuning the double quantum coherence spectra are discussed [52].

The eigenstates of Eq. (41) form exciton bands. For our application we need the lowest three: the ground state $|g\rangle$, single exciton state $|e\rangle$ and double exciton states $|f\rangle$. The diagonalized Hamiltonian then assumes the form:

$$H_0 = E_g|g\rangle\langle g| + \sum_e E_e|e\rangle\langle e| + \sum_f E_f|f\rangle\langle f|, \tag{62}$$

$$V^\dagger = \sum_e V^*_{ge}|e\rangle\langle g| + \sum_{ef} V^*_{ef}|f\rangle\langle e|. \tag{63}$$

The following simulations used a model of three coupled two level systems, and the level scheme is shown in Fig. 1.

We assume the following wavefunction for the entangled photon pair in two beams i and j

$$|\Psi(\tau)\rangle = |0\rangle + \sum_{\mathbf{k}_i,\mathbf{k}_j} f(\mathbf{k}_i,\mathbf{k}_j)a^\dagger_i(\mathbf{k}_i)a^\dagger_j(\mathbf{k}_j)|0\rangle, \tag{64}$$

where $|0\rangle$ is the vacuum state Four beams of two entangled photon pairs $(\mathbf{k}_1,\mathbf{k}_2)$ and $(\mathbf{k}_3,\mathbf{k}_4)$ with $\mathbf{k}_4 = \mathbf{k}_1 + \mathbf{k}_2 - \mathbf{k}_3$ interact with the system as shown in Fig. 8. The signal is defined as the change in the transmitted intensity in mode $\mathbf{k}_4$. The two entangled photon pairs are temporally well separated and $(\mathbf{k}_1,\mathbf{k}_2)$ comes before $(\mathbf{k}_3,\mathbf{k}_4)$. In addition the two photons of each pair are time ordered, $\mathbf{k}_1$ comes before $\mathbf{k}_2$ and $\mathbf{k}_3$ before $\mathbf{k}_4$. We thus have a similar configuration to an impulsive experiment with four short well separated classical fields. Introducing a delay τ_{12} between the photons in the entangled pair $\mathbf{k}_1$ and $\mathbf{k}_2$ (τ_{34} for $\mathbf{k}_3$ and $\mathbf{k}_4$) and a delay $T_{12}/2 + \tau_d + T_{34}/2$ between the two photon pairs. The two entanglement times need to be included in this delay time to guarantee that $\mathbf{k}_1$ and $\mathbf{k}_2$ comes before $\mathbf{k}_3$ and $\mathbf{k}_4$ for all $\tau_d > 0$.

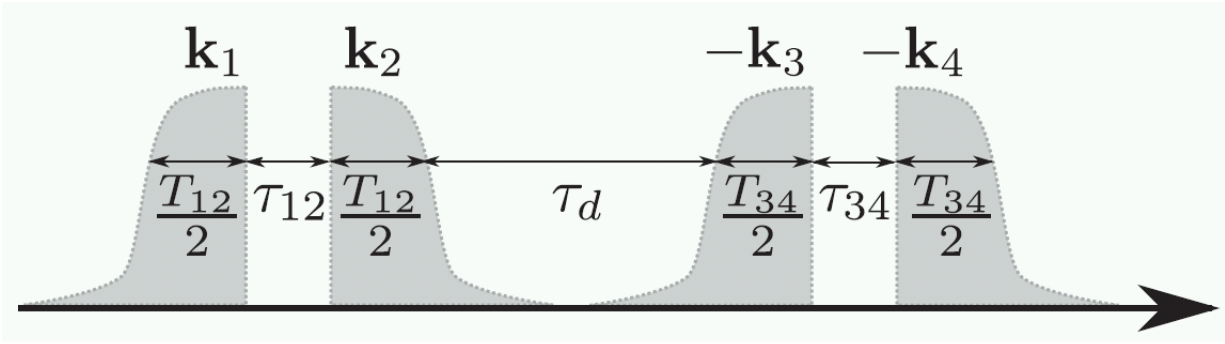

Figure 7: Pulse configuration for the double-quantum-coherence signal [52]. (reprinted with permission. Copyright 2010, American Physical Society.)

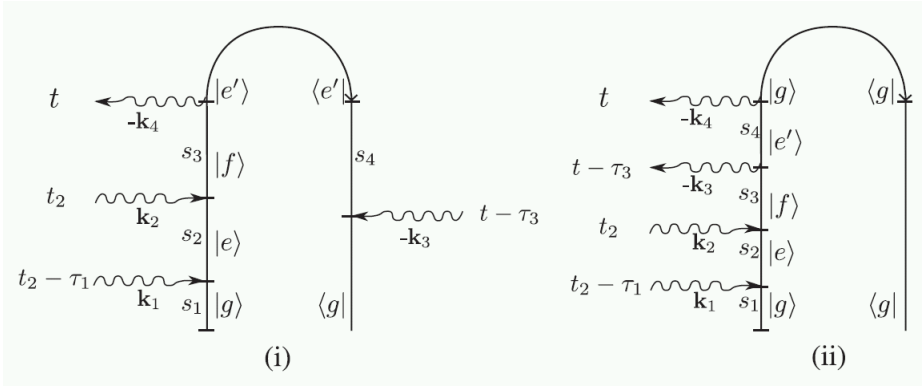

Figure 8: Pathways contributing to the double-quantum-coherence signal at $\mathbf{k}_4 = \mathbf{k}_1 + \mathbf{k}_2 - \mathbf{k}_3$. s_i are the time intervals along the loop, whereas t, t_2, $t - \tau_3$, and $t_2 - \tau_1$ are real, physical time, variables [52]. (reprinted with permission. Copyright 2010, American Physical Society.)

The two contributions to the signal are depicted as CTPL diagrams in Fig. 8. The signal is given by [52]

$$\begin{aligned} S(\Gamma) \quad = \quad & -\frac{1}{\hbar^3}\mathrm{Re}\int_0^\infty \mathrm{d}s_1 \int_0^\infty \mathrm{d}s_2 \int_0^\infty \mathrm{d}s_3 \int_0^\infty \mathrm{d}s_4 \\ & [-\langle\Psi|\hat{E}_3^\dagger(s_1+s_2+s_3-s_4)\hat{E}_4^\dagger(s_1+s_2+s_3)\hat{E}_2(s_1+s_2)\hat{E}_1(s_1)|\Psi\rangle \\ & \qquad \langle V^\dagger(s_1+s_2+s_3-s_4)V^\dagger(s_1+s_2+s_3)V(s_1+s_2)V(s_1)\rangle \\ & +\langle\Psi|\hat{E}_4^\dagger(s_1+s_2+s_3+s_4)\hat{E}^\dagger(s_1+s_2+s_3)_3\hat{E}_2(s_1+s_2)\hat{E}_1(s_1)|\Psi\rangle \\ & \qquad \langle V^\dagger(s_1+s_2+s_3+s_4)V^\dagger(s_1+s_2+s_3)V(s_1+s_2)V(s_1)\rangle]. \end{aligned} \tag{65}$$

The signal may be displayed by the variation with various control parameters of the field wave function. These are denoted collectively as Γ lead to different types of 2D signals.

The photon configuration is depicted in Fig. 7. τ_{12}, τ_{34}, T are positive. We have introduced the complex frequency variables $\xi_{ij} = \omega_{ij} + i\gamma_{ij}$, where $\omega_{ij} = \varepsilon_i - \varepsilon_j$ are the transition frequencies and γ_{ij} are the dephasing rates. In our calculations we set $\gamma_{ij} = \gamma = 1$.

In Fig. 9 we display the 2D signal

$$S(\Omega_{12}, \Omega_{34}) = \int_0^\infty \mathrm{d}\tau_{12} \int_0^\infty \mathrm{d}\tau_{34} S(\tau_{12}, \tau_{34}) e^{-\imath\tau_{12}\Omega_{12} - \imath\tau_{34}\Omega_{34}}, \tag{66}$$

where ω_{eg} resonances are seen along Ω_{12} and ω_{eg} and ω_{fe} on axis Ω_{34}.

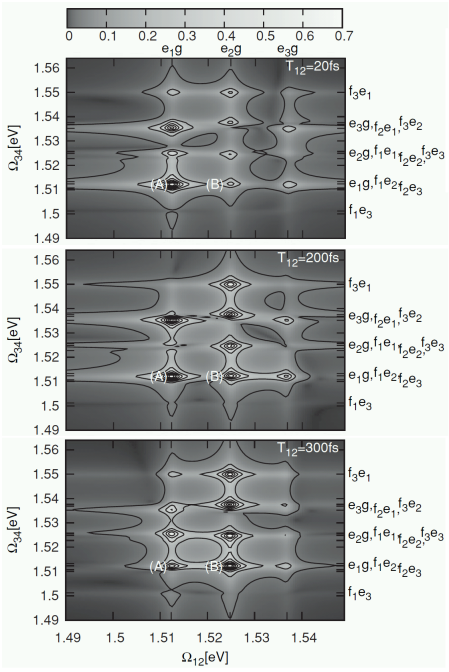

Figure 9: 2D signal for different values of T_{12}. Plots are multiplied by a factor of 1.0 (top), 3.5 (middle), and 6.0 (bottom) [52]. (reprinted with permission. Copyright 2010, American Physical Society.)

By varying T_{12}, we expect an oscillation of the magnitudes of resonances with different frequencies. This is exactly what we see in Fig. 9. We focus on the resonance (A), and on the resonance (B). At T_{12} = 20fs, peak (A) is much stronger (B), however as T_{12} increases the peak height of (A) is much more similar to (B) at T_{12} = 200fs, while at T_{12} = 300fs finally (B) is stronger than peak (A). (Note all plots are normalized to the largest resonance.) The reason for this is that both peaks undergo a sinc like oscillation with a different frequency, it gives us additional control over the spectrum. This can also be true for two partially overlapping resonances for some cases and the entanglement time provides are tool to dissect them. The same effect can be seen for other resonances, where it can be clearly seen that the oscillation frequency is characteristic to each peak. We can analyze the peak oscillations in more detail: (A) is connected to ω_{e_1g} on the Ω_{12} axis and ω_{e_1g} at the other axis, thus actually all three excitonic states contribute and the oscillation of this peak should be a superposition of these three contributions with three different oscillation frequencies $(\omega_{f_ig}/2 - \omega_{e_1g})$.$(B)$ consists of two peaks with ω_{e_2g} on the Ω_{12} axis and $\omega_{f_1e_2}$ or ω_{e_1g} at the Ω_{34} axis. The part connected with ω_{e_1g} on Ω_{34} is similar to (A) connected to all three biexciton states and has parts oscillating with three frequencies $\omega_{f_ig}/2 - \omega_{e_2g}$, the part with ω_{e_1g} on Ω_{34} will oscillate only with $\omega_{f_1g}/2 - \omega_{e_2g}$. Note, that the e state in the oscillation frequency is determined by the Ω_1 axis, if we vary T_{12}, if we vary T_{34} instead, it is determined by the states assigned to the transitions on the Ω_{34} axis.

This example of double quantum coherence 2D spectroscopy of excitons with entangled photon pairs demonstrates that the signal offers improved intensity scaling, relaxed laser bandwidth requirements and additional control of the peaks compared to classical beams.

6.2. Chromophore entanglement induced by coupling to entangled photons; Many-body Collective Resonances in Nonlinear Spectroscopy

The canonical model of the nonlinear optical response assumes that the matter is made out of N noninteracting molecules in the active volume. It is then expected that the contributions made by different molecules to the signals will be additive so that the nonlinear susceptibilities or response functions of the sample are simply given by N times those of a single molecule; the calculation thus reduces to a single body problem [7, 9]. This is no longer the case once

intermolecular interactions are included. Spectra of chromophore aggregates must be calculated in the direct-product space of all molecules. The many-body space size grows exponentially with the number of molecules (for a collection of n-level molecules this is n^N). In perturbative techniques which use weak fields, it is sufficient to consider a subspace of few excitations $m = 1, 2, \cdots$. The number of relevant many-body states in then smaller, i.e. N single excitons and $N(N-1)/2$ two excitons etc. This is a power law rather than exponential scaling.

The above argument is straightforward and intuitive. However it is not so obvious how to rationalize the $\sim N$ scaling for non-interacting molecules had we chosen to work in the N-particle space from the outset. The number of possible paths for the radiation- matter interaction then increases rapidly with N but there must be a massive cancellation in order to recover the final $\sim N$ scaling of the signal. We first give a formal proof for this cancellation. Apart from the physical insight, this provides a starting point for describing many-body effects which result from the elimination of this cancellation. It is clear that the response of interacting molecules should be described in the many body space. We show that this is the case even in the absence of interactions, provided we use entangled photon source fields. These induce entanglement of the molecules; the response of different chromophores is no longer additive and can show collective effects. The proof is very simple if we use the superoperator notation. In this language the nth order response is given by Eq. (15) For clarity we provide the proof for two noninteracting molecules A and B ($N = 2$). We then have $V_\pm = V_\pm^A + V_\pm^B$. The generalization to N molecules is straightforward. This product then factorizes into two terms of the form $\left\langle V_\pm^A(\tau_n)\cdots V_-^A(\tau_1)\right\rangle$. The expectation value of a product of only "minus" operators vanishes identically (since it amounts to the trace of a commutator). The last interaction must be a +. Since this product only contains one + operator, one of these factors, either A or B must therefore vanish. The only surviving terms are when all interactions are either of A or B type, no mixed terms are allowed. This gives twice the response of a single molecule. The same argument applies to N molecules.

We next turn to spectroscopy with quantum fields. When the field-matter interaction is given by Eq. (2), Eq. (14) in the impulsive limit is then replaced by

$$S^{(n)}(\tau_n, \cdots, \tau_1) = \left(\frac{i}{\hbar}\right)^n \left\langle H'_+(\tau_n)H'_-(\tau_{n-1})\cdots H'_-(\tau_1)\right\rangle. \tag{67}$$

A product of superoperators satisfies (see Eq. 29)

$$H'_- = V_+E_- + V_-E_+, \tag{68}$$

$$H'_+ = V_+E_+ + V_-E_-. \tag{69}$$

When H' is factorized into products of matter and field superoperators, Eq. 67 will contain several V_+ operators. If we have at least one + operator for A and one for B, products of terms involving the two molecules now survive and cooperative effects become possible. For classical fields in coherent states $E_- = 0$ and we recover the classical result.

For a model of N noninteracting optically active molecules coupled to classical fields, the many-body matter density matrix is a direct product of the N density matrices of the individual particles at all times and any responses, be it linear or nonlinear is simply given by N times the response of a single molecule. The entire analysis can be made in the single molecule Hilbert space, and the calculation becomes a single-body problem. Had we chosen to describe the response in the many-body Hilbert space, the response will have a considerably larger number of pathways. We can generally write $\chi = \chi^A + \chi^B + \chi^{AB}$. In the first (second) term all dipole interactions occur in the $A(B)$ space. These are the individual responses of molecules A and B. The last term represents many-body interference and contains the large number of pathways in which some interactions are with A and the others are with B. ¿From the above argument we know what all of these terms must sum to zero and we need not consider this term at all for noninteracting molecules driven by classical fields. However, once we use entangled photons and let them interact with the molecules, the entire system of two molecules and the photon field become entangled and the density matrix may no longer be factorized, even if the molecules do not interact. Under these conditions the cooperative term χ^{AB} no longer vanished, and we must describe the problem in the many-body Hilbert space. The additional many-body pathways thus provide entangled-induced contributions and have been shown to give rise to new collective resonances [53]. The shaping of classical pulses may also be used to affect signals. However, it is in principle impossible to induce χ^{AB} with classical pulses. Photon entanglement is fundamentally different from pulse shaping and provides a different level of control over the response.

7. Acknowledgement

We gratefully acknowledge the support of the National Science Foundation Grant (No. CHE-0745892) and the Chemical Sciences, Geosciences and Biosciences Division, Office of Basic Energy Sciences, Office of Science, US Department of Energy. We wish to thank Drs. Vladimir Chernyak, Adam Cohen, Oleksiy Roslyn's, Upendra Harbola, and Marten Richter who made major contributions to the work covered in this article.

8. References

[1] R.P. Feynman and A.R. Hibbs, Quantum Mechanics and Path Integrals (McGee's Hill, New York, 1965).
[2] J. Itatani, J. Levesque, D. Zeidler, H. Niikura, H. Pepin, J.C. Kieffer, P.B. Corkum, and D.M. Villeneuve, Nature 432 (2004) 867; H.J. Worner, J.B. Bertrand, D.V. Kartashov, P.B. Corkum, D.M. Villeneuve, Nature 466 (2010) 604.
[3] T.J. Dunn, I.A. Walmsley, and S. Mukamel, Phys. Rev. Lett. 74 (1995) 884.
[4] F. Mintert, A.R.R. Carvalho, M. Kus, and A. Buchleitner, Phys. Rep. 415 (2005) 207.
[5] S. Lloyd, Science 261 (1993) 1569.
[6] V. Vedral, M.B. Plenio, M.A. Rippin, and P.L. Knight, Phys. Rev. Lett. 78 (1997) 2275.
[7] S. Mukamel, Principles of Nonlinear Optical Spectroscopy (Oxford University Press, New York, 1995).
[8] J. Rammer, Quantum Transport Theory (Westwiew Press, Colorado, 2008).
[9] M. Scully and M. Zubairy, Quantum Optics (Cambridge University Press, Cambridge, 1997).
[10] S. Mukamel, Annu. Rev. Phys. Chem. 51 (2000) 691.
[11] V. Chernyak, N. Wang, and S. Mukamel, Phys. Rep. 263 (1995) 213.
[12] U. Harbola and S. Mukamel, Phys. Rep. 465 (2008) 191.
[13] C.A. Marx, U. Harbola, and S. Mukamel, Phys. Rev. A 77 (2008) 022110.
[14] O. Roslyak and S. Mukamel, Mol. Phys. 107 (2009) 265.
[15] K.C. Chou, Z.-B. Su, B.-L. Hao, and L. Yu, Phys. Rep. 118 (1985) 1.
[16] L.V. Keldysh, Sov. Phys. J. 20 (1965) 1018.
[17] R. Mills, Propagators for many-particle systems; an elementary treatment (New York, Gordon and Breach, 1969).
[18] A.E. Cohen and S. Mukamel, Phys. Rev. Lett. 91 (2003) 233202.
[19] R. Glauber, Quantum Theory of Optical Coherence: Selected Papers and Lectures (Wiley VCH, Weinheim, 2007).
[20] Y. Tanimura and S. Mukamel, J. Chem. Phys. 99 (1993) 9496.
[21] A.J. Stone, The Theory of Intermolecular Forces (Clarendon Press, Oxford, 1996).
[22] P.W. Milonni, The Quantum Vacuum: An Introduction to Quantum Electrodynamics (Academic Press, New York, 1994).
[23] H.B.G. Casimir and D. Polder, Phys. Rev. 73 (1948) 360.
[24] A.D. McLachlan, Proc. R. Soc. London, Ser. A 271 (1963) 387; 274 (1963) 80.
[25] J. Mohanty and B.W. Ninham, Dispersion Forces (Academic Press, New York, 1976).
[26] U. Harbola and S. Mukamel, Phys. Rev. A 70 (2004) 052506.
[27] D. Abramavisius, B. Palmieri, D. Voronine, F. Sanda, and S. Mukamel, Chem. Rev. 109 (2009) 2350.
[28] W.M. Zhang, T. Meier, V. Chernyak, and S. Mukamel, J. Chem. Phys. 108 (1998) 7763.
[29] G.S. Engel, T.R. Calhoun, E.L. Read, T.K. Ahn, T. Mancal, Y.C. Cheng, R.E. Blankenship, and G.R. Fleming, Nature (London) 446 (2007) 782.
[30] E. Collini and G.D. Scholes, Science 323 (2009) 369.
[31] M. Mohseni, P. Rebentrost, S. Lloyd, and A. Aspuru-Guzik, J. Chem. Phys. 129 (2008) 174106.
[32] V. Chernyak and S. Mukamel, J. Opt. Soc. Am. B 13 (1996) 1302.
[33] M. Combescot, O. Betbeder-Matibet, and F. Dubin, Phys. Rep. 463 (2008) 215.
[34] S. Mukamel, J. Chem. Phys. 132 (2010) 241105.
[35] W.M. Zhang, T. Meier, V. Chasrnyak, and S. Mukamel, Philos. Trans. R. Soc. London, Ser. A 356 (1998) 405.
[36] Y. Zhao, T. Meier, W. Zhang, V. Chernyak, and S. Mukamel, J. Phys. Chem. 103 (1999) 3954.
[37] S. Mukamel, R. Oszwaldowski, and L. Yang, J. Chem. Phys. 127 (2007) 221105.
[38] F.C. Spano and S. Mukamel, Phys. Rev. Lett. 66 (1991) 1197.
[39] J.A. Leegwater and S. Mukamel, Phys. Rev. A 46 (1992) 452.
[40] S. Mukamel, Molecular Nonlinear Optics, J. Zyss, Ed. (Academic Press, New York, 1994).
[41] W. Zhang, V. Chernyak, and S. Mukamel, J. Chem. Phys. 110 (1999) 5011.
[42] H. Haug and A.P. Jauho, Quantum Kinetics in Transport and Optics of Semiconductors (Springer-Verlag, Berlin, Heidelberg, 1996).
[43] D.A. Lang, The Raman Effect: A unified Treatment of the Theory of Raman Scattering by Molecules. (Wiley, 2002).
[44] O. Roslyak and S. Mukamel, Opt. Express 17 (2009) 1093.
[45] A. Peer, B. Dayan, A.A. Friesem, and Y. Silberberg, Phys. Rev. Lett. 94 (2005) 073601.
[46] D. Lee and T. Goodson, J. Phys. Chem. B 110 (2006) 25582.
[47] B.E.A. Saleh, B.M. Jost, H.-B. Fei, and M.C. Teich, Phys. Rev. Lett. 80 (1998) 3483.
[48] S. Friberg, C. Hong, and L. Mandel, Opt. Commun. 54, 311 (1985).
[49] L. Yang and S. Mukamel, Phys. Rev. B 77 (2008) 075335.
[50] J. Kim, S. Mukamel, and G. D. Scholes, Acc. Chem. Res. 42 (2009) 1375.
[51] L. Yang, T. Zhang, A.D. Bristow, S.T. Cundiff, and S. Mukamel, J. Chem. Phys. 129 (2008) 234711.
[52] M. Richter and S. Mukamel, Phys. Rev. A 82, 013820 (2010).
[53] A. Muthukrishnan, G.S. Agarwal, and M.O. Scully, Phys. Rev. Lett. 93 (2004) 093002.